Study of $B \to (\chi_{c1}\gamma)K$ Decay in Belle II

Debjit Ghosh

Reg. No: MS15199

A dissertation submitted for the fulfillment of BS-MS dual degree in Science

Under the guidance of

Dr. Vishal Bhardwaj

Indian Institute of Science Education and Research, Mohali

June 2020

Certificate of Examination

This is to certify that the dissertation titled **"Study of $B \to (\chi_{c1}\gamma)K$ decay in Belle II"** submitted by **Debjit Ghosh** (Reg. No. MS15199) for the partial fulfillment of BS-MS dual degree programme of the Institute, has been examined by the thesis committee duly appointed by the Institute. The committee finds the work done by the candidate satisfactory and recommends that the report be accepted.

Dr. Harvinder Kaur Jassal Dr. Ambresh Shivaji Dr. Vishal Bhardwaj
(Supervisor)

Dated: June 30, 2020

Declaration

The work presented in this dissertation has been carried out by me under the guidance of Dr. Vishal Bhardwaj at the Indian Institute of Science Education and Research Mohali.

This work has not been submitted in part or in full for a degree, a diploma, or a fellowship to any other University or Institute. Whenever contributions of others are involved, every effort is made to indicate this clearly, with due acknowledgment of collaborative research and discussions. This thesis is a bonafide record of original work done by me, and all sources listed within have been detailed in the bibliography.

Debjit Ghosh
(Candidate)

Dated: June 30, 2020

In my capacity as the supervisor of the candidate's project work, I certify that the above statements by the candidate are accurate to the best of my knowledge.

Dr. Vishal Bhardwaj
(Supervisor)

Acknowledgment

I would like to express my sincere gratitude to my thesis supervisor, Dr. Vishal Bhardwaj, for his excellent guidance, encouragement, and support that made it possible to do my MS thesis project. His outgoing and generous personality always makes me comfortable. His insight into the topic has always helped me and motivated me to understand the subject better. Every time he has tried to teach me not to chase after the result, instead, I must comprehend the hidden beauty of the analysis tools. But even now, I make the same mistake repeatedly. I would like to thank my thesis committee members: Dr. Ambresh Shivaji and Dr. Harvinder Kaur Jassal, for their valuable comments on my thesis.

I wish to thank my senior, Rajesh Maiti, for his eagerness to help me out and encourage me to do hard work. I am fortunate to have him on my team. No matter at what time, he is always ready to troubleshoot my problem. I want to thank Ph.D. student, Sourav Patra, to allow me to use his tagging tools in my background study.

I sincerely thank the Belle II collaboration to provide me with a platform to do all my computational work and to explore the beauty of the experimental particle physics. I am also thankful to the Indian Grid Certification Authority(IGCA) to give me the grid access.

I am grateful to Dr. Abhishek Chowdhuri for his support and kindness. He always helped me whenever I am in trouble. His teaching excellence motivates me. I consider myself lucky to work under Prof. P.K. Panigrahi in my first two summer projects. His passion and unique ways of doing research always amaze me. I wish to thank him for allowing me to pursue research and giving his helping hand when necessary.

I would like to acknowledge the efforts of the mess workers and housing staff of IISER, who work tirelessly to make us feel at home. I would like to give a special thanks to Mr. Kamol Halder, the person-in-charge of my broadband provider. He always gives me prior importance to make my work go smoothly during the lockdown.

I am genuinely grateful to Adarsh, Amit, Anubhav, Apoorv, Debanjan, Gaurav, Ishan, Milind, Nikhil, Nilangshu, Paresh, Rohit, Sohit, Satyam, Sumith, Swastik, and Vivek for their excellent company and invaluable support. It has been an enjoyable

and exciting hostel life that I will cherish throughout my life.

I acknowledge IISER Mohali for providing me with the best infrastructures and environment for carrying out my BS-MS programme. It gave me the opportunity to meet with beautiful people and connect me with various cultures in our country. I am thankful to the Department of Science and Technology's (DST) Innovation in Science Pursuit for Inspired Research (INSPIRE) Scholarship that provides me with financial help for the last five years.

I am deeply grateful to my childhood friends Arindam, Ayan, and Subhajit, for their continuous support that makes my life beautiful. Lastly, I would like to thank my father, my mother, and my brother and sister, who are my pillars of support. Their endless help made me what I am and give me the confidence to chase after my dreams.

Debjit Ghosh
MS15199

List of Figures

List of Tables

Symbol

$\Upsilon(nS)$	Upsilon(nS) mesons	B	B meson
D	D meson	J/ψ	$\psi(1S)$ meson
$\psi(2S)$	$\psi(2S)$ meson	K	Kaon
π	Pion	e	Electron
μ	Muon	τ	Tau
ν_e	Electron neutrino	ν_μ	Muon neutrino
ν_τ	Tau neutrino	ℓ	Lepton
p	Proton	d	Deuteron
γ	Photon	q	Quark
u	Up quark	d	Down quark
s	Strange quark	c	Charm quark
t	Top quark	b	Bottom quark
E_{beam}	Beam Energy in CM frame	M_{bc}	Beam constraint Mass
Γ	Decay width	$\mathcal{B}$	Branching fraction

Acyonyms

ARICH	Aerogel Ring Imaging Cherenkov Detector
BASF2	Belle II Analysis Software Framework
CDC	Central Drift Chamber
CM	Center of Mass
COPPER	COmmon Pipeline Platform for Electronic Readout
DAQ	Data Acquisition
DEPFET	Depleted P−channel Field Effect Transistor
DSSD	Double−sided Silicon Strip Detector
ECL	Electromagnetic Calorimeter
GDL	Global Decision Login
HAPD	Hybrid Avalanche Photon Detector
HER	High Energy Ring
HLF	High Level Trigger
IP	Interaction Point
IR	Interaction Region
KLM	K_L^0 and μ Detector
LER	Low Energy Ring
MC	Monte Carlo
MCP−PMT	Micro Channel Plate−Photo Multiplier Tube
NbTi/cu	Niobium Titanium and Copper Wiring
PID	Particle Identification Detector
PDF	Probability Distribution Function
PDG	Particle Data Group
PXD	Pixel Detector
RICH	Ring Imaging Cherenkov Detector
ROI	Region of Interest
S10C	SAE−AISI 1010 Carbon steel
SiPm	Silicon Photo Multiplier
SVD	Silicon Vertex Detector
TOF	Time of Flight
TOP	Time of Propagation Detector
WLS	Wavelength Shifting

Contents

Abstract

The thesis aims to perform a sensitivity study of the $B \to X(3823)K\pi$ in the Belle II data set. If $X(3823)$ is $\psi(1\,^3D_2)$ state with $J^{PC} = 2^{--}$, like χ_{c2} ($J^{PC} = 2^{++}$), its branching fraction of three body decay mode $B \to (\chi_{c1}\gamma)K\pi$ will be higher than its two body decay mode $B \to (\chi_{c1}\gamma)K$. We performed signal Monte Carlo study for the two and three body decay modes and estimated the reconstruction efficiency of $\psi(2S)$, $X(3823)$, and $X(3872)$. We improved the resolution of $M(\chi_{c1}\gamma)$ using the γ energy scaling by forcing ΔE to be zero. We planned to do the background study in order to estimate the sensitivity. Due to the current COVID-19 scenario, we could not complete this task. However, we do provide the expected signal efficiency for the decay mode of interest.

Chapter 1

Introduction

The elementary world is divided into two main categories: fermions (fractional spins) and bosons (integral spins). Baryons and leptons are fermions, whereas mesons and force mediators are bosons. Hadrons and leptons (ℓ) are classified in three generations, higher the generation higher its mass. Each lepton has its neutrino. Moreover, Hadrons are made of quarks, and there are six quarks, among which two quarks are grouped in each generation. Description (based on Particle Data Group [Zyla 20]) of different types of elementary particles and force mediators are given in table 1.1 and table 1.2, respectively.

1.1 Mesons

Mesons ($q\bar{q}$) are made of one quark and one antiquark. This structure makes meson a boson, while quark is fermion. Meson can be charged (like $\pi^{\pm}$, $K^{\pm}$, ...) or neutral (like π^0, K^0, ...) depending on the combination of quark-antiquark charges. This configuration of quark-antiquark pair make meson a spin triplet or spin singlet. Quarkonium ($q\bar{q}$) is a particular type of meson that consists of a quark and antiquark of the same kind, like charm or bottom.

Generation	**Quark**	**Mass**	**Charge** (e)
First	Up (u)	$2.16^{+0.49}_{-0.26}\,\mathrm{MeV}/c^2$	$+\frac{2}{3}$
	Down (d)	$4.67^{+0.48}_{-0.17}\,\mathrm{MeV}/c^2$	$-\frac{1}{3}$
Second	Charm (c)	$1.27 \pm 0.02\,\mathrm{GeV}/c^2$	$+\frac{2}{3}$
	Strange (s)	$93^{+11}_{-5}\,\mathrm{MeV}/c^2$	$-\frac{1}{3}$
Third	Top (t)	$172.76 \pm 0.30\,\mathrm{GeV}/c^2$	$+\frac{2}{3}$
	Bottom (b)	$4.18^{+0.03}_{-0.02}\,\mathrm{GeV}/c^2$	$-\frac{1}{3}$
Generation	**Lepton**	**Mass**	**Charge** (e)
First	Electron (e)	$0.511\,\mathrm{MeV}/c^2$	-1
	Electron Neutrino (ν_e)	$< 1.1\,\mathrm{eV}/c^2$	0
Second	Muon (μ)	$105.658\,\mathrm{MeV}/c^2$	-1
	Muon Neutrino (ν_μ)	$< 0.19\,\mathrm{MeV}/c^2$	0
Third	Tau (τ)	$1776.86 \pm 0.12\,\mathrm{MeV}/c^2$	-1
	Tau Neutrino (ν_τ)	$< 18.2\,\mathrm{MeV}/c^2$	0

Table 1.1: Description of elementary particles

Force	**Mediator**
Strong	Gluons
Electromagnetic	Photon
Weak	$W^\pm$, Z^0 bosons
Gravitation	Graviton (unobserved)

Table 1.2: List of elementary forces

$\Upsilon(1S)$ is a quarkonium meson with bottom quark. In 1977, at Fermilab, it was first observed at $9.5\,\mathrm{GeV}/c^2$ mass in 400 GeV proton-nucleus collision [Herb 77]. Later, higher states of Υ was found, and $\Upsilon(4S)$ becomes the perfect resonance to produce $B\bar{B}$ pair. $B\bar{B}$ is the pair of B mesons with its anti-particle. B mesons are made of a heavy bottom anti-quark and a light quark like up, down, strange, and charm. Neutral B mesons pair ($B^0-\bar{B}^0$ or $B^0_s-\bar{B}^0_s$) shows flavor oscillations, which means they spontaneously transform from particle to its anti-particle and vice-versa. SuperKEKB accelerator operates at $\Upsilon(4S)$ resonance to produce a large number of $B\bar{B}$ pairs.

1.2 Charmonium

Quarkonium with charm quark is known as charmonium ($c\bar{c}$). Each $c\bar{c}$ state can be labeled as $^{2S+1}L_J$ with quantum number J^{PC} , where L is the orbital angular

momentum and S is the spin angular momentum.

Parity, $P = (-1)^{L+1}$
Charge parity, $C = (-1)^{L+S}$
Total angular momentum, $J = |L + S|$ to $|L - S|$

The potential that explains the charmonium system has two parts: Firstly, it has a dominating short distance coulomb like term which comes from inter-quark force (gluon exchange), and secondly, a dominating large distance linear term due to confinement [Olsen 16].

$$V(r) = -\frac{A}{r} + Br$$

where r is the distance and A, B are the proportionality constants. Several properties are observed by inspecting decay patterns of the charmonium states.

- Electromagnetic transition: Prediction of dominating EM transition provides satisfying experimental results like ${}^3P_J \leftrightarrow {}^3S_1$ (e.g. $\chi_{c1} \rightarrow J/\psi$ transitions is observed in our study).
- Transition involves the emission of light hadrons like $\psi(2S) \rightarrow J/\psi\pi^+\pi-$ or $\psi(2S) \rightarrow J/\psi\pi^0$ which can be predicted from the multi-pole expansion of the gluonic field.
- Weak decays of heavy quarks like $J/\psi \rightarrow \bar{D}_s e^+ \nu_e$.
- Quark-antiquark annihilation into photons or gluons like $J/\psi \rightarrow ggg \rightarrow hadrons$

1.2.1 Charmonium Production

In B-factory, charmonium is produced in many ways. The four significant ways are listed below:

1. ***B* meson decay**: Through weak decay, charmonium state with any quantum number can be produced from B mesons in $B \rightarrow c\bar{c}\,K$ channel.

2. **Two photon production**: Electron and positron annihilate at high energy to produce charmonium state (with even $J^{PC} = 0^{-+}$, 0^{++}, 2^{-+}, and 2^{++}) through two virtual photons.

3. **Initial state radiation**: Electron and positron annihilate to produced charmonium state and radiated photon. Only $J^{PC} = 1^{--}$ states are allowed to create this way.

4. **Double state radiation**: Electron and positron annihilate to produce pair charmonium production with opposite charge parities.

1.3 Charmonium like XYZ mesons

The XYZ mesons tend to decay to daughter particles, which contain heavy quarks like a charm or a bottom quark (or antiquark). Their properties (mass, width, decay rate, ...) do not overlap with the known mesons and baryon states. In-fact, these types of unconventional states were predicted a long time back, even in the original Gell Mann's paper [Gell-Mann 64]. After almost forty years later, Belle Collaboration first observed a charmonium-like unconventional state in 2003 and named it $X(3872)$ (we will talk about it later). Currently, the number of this kind increases a lot, thanks to the charmonium spectroscopy, because most of the XYZ mesons are found while studying charmonium particles. That's why charmonium spectroscopy is crucial to understand these new states.
Over the years, many theories like multiquark, charmonium hybrid, and threshold effect try to explain these new states. Let's take a brief look at these theories (for better understanding, please read Olsen *et al.* review papers [Godfrey 08] [Olsen 16]).

1.3.1 Multiquark

As its name says, multiquark has a more complex quark structure than 3-quark baryons (qqq) or 2-quark mesons ($q\bar{q}$). The multiquark structure can form tetraquark mesons, pentaquark baryons, or six-quark H di-baryons. $X(3872)$ is predicted as a molecular state [Swanson 06] or a tetraquark [Maiani 05]. The Molecular state is

a loosely bound structure of two charmed mesons. Exchange of pions at large distance or gluons at short distance binds these two charmed mesons. As it is loosely bound, it acts as a free decay state [Törnqvist 94] [Ericson 93]. On the other hand, tetraquark has different decay properties. Diquark anti-triplets are formed from two quarks triplet. As they are not color-singlet, they interact with anti-color anti-diquark to produce this tetraquark.

1.3.2 Charmonium Hybrid

Excited gluonic degree of freedom makes a meson state hybrid. Lattice QCD [Isgur 85] provides the quantum number structure (J^{PC}) for these states. While the lowest adiabatic surface in their model predicts conventional charmonium state, the excited adiabatic surface leads us to the possible quantum number for lowest mass hybrids ($J^{PC} = 0^{+-}$, 0^{-+}, 1^{++}, 1^{--}, 1^{+-}, 1^{-+}, 2^{+-}, 2^{-+}, but 0^{-+}, 1^{-+}, 2^{+-} are not possible for $c\bar{c}$ states). EM transition, hadronic transition are possible decay pattern of the charmonium hybrid states.

1.3.3 Threshold Effect

The threshold of DD^*, D^*D^* , DD_1 and D^*D_1 at center mass energy 3872 MeV, 4020 MeV, 4287 MeV, and 4430 MeV respectively affect the $c\bar{c}$ state resonance. Strong interaction of pion exchange can lead to molecular state or repulsive interaction causes shifts in their masses [Close 08]. Below $D\bar{D}$ threshold, theoretical prediction agrees very well with the experimental result. However, above one finds a discrepancy between experimental result and theoretical predictions.

1.4 X(3872)

In 2003, Belle collaboration first observed a narrow peak of $X(3872)$ state in $B \to K\pi^+\pi^- J/\psi$ decay where $X(3872) \to J/\psi\pi^+\pi^-$ ([Choi 03]). Soon after, CDF [Acosta 04],

D0 [Abazov 04], BaBar [Aubert 05], LHCb [Aaij 12] and CMS collaboration [Chatrchyan 13] confirmed this new state (mass=$3871.69 \pm 0.17\,\mathrm{MeV}/c^2$ [Zyla 20]). Before 2003, the existence of a $D\bar{D}^*$ bound state is predicted near $3870\,\mathrm{MeV}/c^2$ with $J^{PC} = 0^{-+}$ and 1^{++} [Törnqvist 94]. Later, investigation held strong evidence of J^{PC} to be 1^{++} [Aaij 13] [Abulencia 07]. However, the problem rises with its isospin. $X \to \pi^+\pi^- J/\psi$ suggests isospin (I) of X to be 0 or 1 [Abulencia 06] [Choi 11]. For $I = 0$, $X \to \rho J/\psi$ will violate isospin symmetry, whereas, for $I = 1$, neutral $X(3872)$ must have its charged partner. As its mass is near $D\bar{D}^*$ bound state, it is more likely that the charged partner will decay to $D\bar{D}^*$ bound state, and eventually, giving broader mass distribution. Later, studies of $X(3872) \to \omega J/\psi$ decay by Belle [Abe 05] and BaBar [del Amo Sanchez 10] [Aubert 08] show strong evidence against $I = 1$.

Residing $X(3872)$'s mass very close to $D^0\bar{D}^{*0}$ ($3871.84 \pm 0.27\,\mathrm{MeV}/c^2$ [Zyla 20]), it is suggested as a molecular state [Swanson 06]. However, LHCb [Aaij 12] and CMS [Chatrchyan 13] in pp collision, and Belle [Bhardwaj 11] and BaBar [Aubert 09] in $X(3872) \to J/\psi\gamma$ decay show discrepancy results for $X(3872)$ to become a molecular loosely bound state.

χ'_{c_1} is the possible charmonium state ($2\,^3P_1$) for $X(3872)$. The strength of this suggestion increases as both of them have the same quantum number and small expected mass difference [Barnes 05]. However, for charmonium state, $X(3872) \to \rho J/\psi$ decay is isospin and OZI violating.

Apart from the charmonium hybrid or hydro-charmonium model, Maiani *et al.* [Maiani 05] tetraquark model of $X(3872)$ has become a reliable prediction after the discovery of $Z_c(3900)^{\pm,0}$, a possible charged partner of $X(3872)$.

All the above discussions give an idea that $X(3872)$ is a captivating candidate in particle physics in the 21^{st} century. Here, in our study, we are searching for its C-odd partner, which has the potential to decay to $\chi_{c1}\gamma$ [Bhardwaj 13a].

1.5 X(3823)

In 1994, the E705 experiment of $J/\psi\pi^+\pi^-$ decay channel first observed a peak at the mass $3836 \pm 13\,\mathrm{MeV}/c^2$ with width $\Gamma = 24 \pm 5$ MeV [Antoniazzi 94]. One expects it to be the $\psi(1\,^3D_2)$ state, as the other D-wave spin triplets, i.e., $1\,^3D_1$ and $1\,^3D_3$ are suppressed by G-parity[1] and OZI allowed opened channel. Further, its mass falls in the range of the expected mass of $1\,^3D_2$ (having $J^{PC} = 2^{--}$), $3.810 - 3.840\,\mathrm{GeV}/c^2$ [Godfrey 85] [Kwong 87] [Ebert 03] [Eichten 04] [Blank 11]. If this new state was $\psi(2D)$, we should have seen it in BaBar, Belle, CDFs. However, this suggests that it was not $\psi(2D)$ state.

After 19 years, in 2013, Belle showed the evidence of a narrow peak that decays to $\chi_{cJ}\gamma$ in $B \to \chi_{cJ}\gamma K$ channel [Bhardwaj 13a]. Their measured mass is $3823.1 \pm 1.8(\mathrm{stat}) \pm 0.7(\mathrm{syst})$ MeV$/c^2$ with 3.8σ (significance), and its branching fraction[2] $\mathcal{B}[B^\pm \to X(3823)\,K^\pm]\,\mathcal{B}[X(3823) \to \chi_{c1}\,\gamma] = 9.7 \pm 2.8 \pm 1.1 \times 10^{-6}$.

Later, in 2015 BESIII confirmed this new state in their reconstruction spectrum of $\chi_{c1}\gamma$ in $e^-e^+ \to \pi^+\pi^-\gamma\chi_{c1}$ channel with a mass of $3821.7 \pm 1.3(\mathrm{stat}) \pm 0.7(\mathrm{syst})\mathrm{MeV}/c^2$ and width of 16 MeV [Ablikim 15]. In each case, $X(3823)$ has a good agreement with $\psi(1\,^3D_2)$ state, having $J^{PC} = 2^{--}$. Even, the theoretical calculation of the upper limit ratio of $\frac{\mathcal{B}[X(3823)\to\chi_{c2}\,\gamma]}{\mathcal{B}[X(3823)\to\chi_{c1}\,\gamma]}$ matches with both experimental values, Belle($<$ 0.40) and BESIII ($<$ 0.42) [Eichten 02] [Ebert 03] [Ko 97] [Qiao 97]. Recently, LHCb has seen $X(3823)$ decay into $J/\psi\pi^+\pi^-$ along with measuring its width to be 5.2 MeV at 90% C.L. [Aaij 20]. If one uses their result along with Belle, then one gets $\frac{\mathcal{B}(X(3823)\to J/\psi\pi^+\pi^-)}{\mathcal{B}(X(3823)\to\chi_{c1}\gamma)} = (2.9 \pm 5.7)\%$. This further suggests it to be $\psi(1\,^3D_2)$.

In the Belle paper Ref.[Abe 02, Bhardwaj 16], it shows two body decay of B mesons to χ_{c2} is suppressed. However, the study of the differential branching fraction [Abe 02] [Aubert 03] suggests that χ_{c2} tends to decay as multi body channel. Similar to χ_{c2} ($J^{PC} = 2^{++}$), if $X(3823)$ has the quantum number $J^{PC} = 2^{--}$, its two body decay to $B \to \psi(2D)\,K$ is suppressed while its three body decay might be enhanced. An initial study was done by Belle and presented in a conference where they look for $B^0 \to$

[1] G-parity, $G = (-1)^{L+S+I}$

[2] Branching fraction is the ratio of the number of a particular daughter particle produced to the number of decays of all particles.

$X(3823)(\rightarrow \chi_{c1}\gamma)K^*(\rightarrow K^+\pi^-)$ decay mode [Bhardwaj 13b]. The result shows the ratio of the branching fraction of two and three body decay mode, $\frac{\mathcal{B}[B^0\rightarrow X(3823)K^+\pi^-]}{\mathcal{B}[B^+\rightarrow X(3823)K^+]} = 2.5 \pm 1.0(\text{stat})$.

Our motivation is to check the sensitivity of two and three body decays, as mentioned above in Belle II and do a feasibility study. This also reflects the fact how the charmonium spectroscopy becomes a fascinating tool to probe these new states, which are predicted long back but remain dormant in our experimental particle physics world.

A List of particles (excluding lepton pair $e^{\pm}$ and $\mu^{\pm}$) related to our study is provided in table 1.3. In chapter 2, we will briefly discuss various fundamental sections of the Belle II detector. Chapter 3 is the main section, where we will discuss our analysis tools. Further, results from our analysis are provided in chapter 4.

Particles	**PDG mass**(MeV/c^2)	$\boldsymbol{I^G(J^{PC}}$ **or** $\boldsymbol{J^P)}$ or $\boldsymbol{I(J^P)}$
$\Upsilon(4S)$	10579.4 ± 1.2	$0^-(1^{--})$
$B^{\pm}$	5279.34 ± 0.12	$\frac{1}{2}(0^-)$
B^0, $\bar{B}^0$	5279.65 ± 0.12	$\frac{1}{2}(0^-)$
$\psi(2S)$	3686.10 ± 0.06	$0^-(1^{--})$
$X(3872)$	3871.69 ± 0.17	$0^+(1^{++})$
$X(3823)$	3822.2 ± 1.2	$0^-(2^{--})$
χ_{c1}	3510.67 ± 0.05	$0^+(1^{++})$
J/ψ	3096.900 ± 0.006	$0^-(1^{--})$
$K^{\pm}$	493.677 ± 0.016	$\frac{1}{2}(0^-)$
$\pi^{\pm}$	139.57039 ± 0.0001	$1^-(0^-)$

Table 1.3: List of particles involved in our study (descriptions are taken from Particle Data Group [Zyla 20])

Chapter 2

Experimental Setup

Record-breaking luminosity[1] accomplishment of B-factory, the KEKB accelerator, and Belle detector are amazingly successful to their goal of discovering New Physics phenomena. Verification of Kobayashi-Mashawa theory, which reflects CP violation, pushes Belle to its zenith. This marvelous B-factory is located at the High Energy Accelerator Research Organization, KEK in Japan.

2.1 Super KEKB Accelerator

Super KEKB accelerator (2010-present) is an upgraded version of the KEKB accelerator (1998-2010). It is an electron-positron (e^-e^+) collider and operates at the center of mass energy $\sqrt{s} = 10.58\,\text{GeV}$, which is equal to the mass of $\Upsilon(4S)$. It has two rings with asymmetric energies, such that, the energy of the high energy ring (HER, containing electron) is 7 GeV, and the energy of the low energy ring (LER, containing positron) is 4 GeV. The targeted peak luminosity of Super KEKB is $8 \times 10^{35}\,\text{cm}^{-2}\,\text{s}^{-1}$, which is almost 40 times higher than KEKB's luminosity ($2.018 \times 10^{34}\,\text{cm}^{-2}\,\text{s}^{-1}$). The main plan to achieve this high luminosity is the "Nano-Beam scheme" [Kou 19] that involves the minimization of vertical beta function[2]. The asymmetric energy between

[1] Luminosity is the ratio of the rate of detecting particle to the interaction cross-section.

[2] Here, it is related to the transverse size of the beam at IP

HER and LER provides Lorentz boost to allow measurement of time-dependent CP symmetry breaking. It will also help to study charmonium spectroscopy and New Physics phenomena including dark matter.

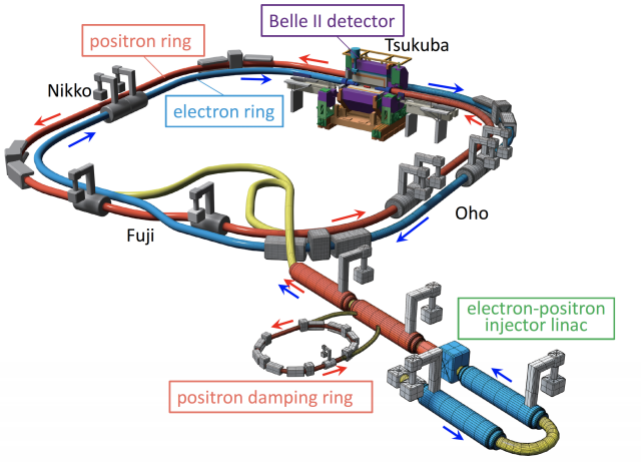

Figure 2.1: Schematic diagram of Super KEKB

2.2 Belle II Detector

Operation at $\Upsilon(4S)$ resonance produces a large amount of B-mesons pairs (B^+B^-, $B^0\bar{B}^0$, ...), that's why Belle II is called a B-factory. Belle II is the sixth B-factory after CLEO, BaBar, Belle, HERA-B, and LHC-b. Heavy particles often have a shorter lifespan as it quickly decays to its lighter daughter particles. As a result, detector are designed to measure various physical properties of these final daughter particles precisely. In this section, a very brief explanation is given for different significant parts of Belle II detector[3]. Interested person must read the Belle II design report [Abe 10] and Belle II physics book [Kou 19] for a detailed explanation.

2.2.1 Interaction region

The interaction region (IR) is designed to achieve a small β function, which can be accomplished by a shorter distance between the final quadrupole magnet and IP. IR

[3]All images in this chapter are taken from SuperKEKB, Belle II sites, and ref. [Abe 10], [Kou 19]

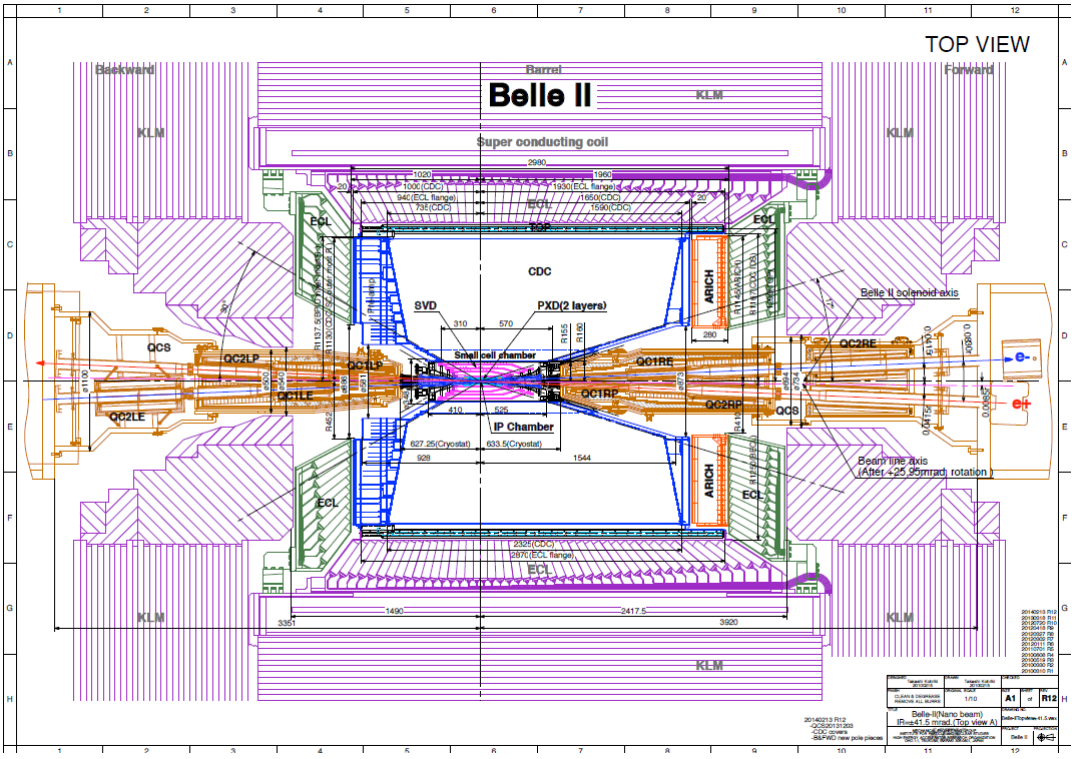

Figure 2.2: Belle II Detector

is composed of superconducting or permanent quadrupole IR magnets and vacuum chambers. IR magnets provide the final focusing mechanism of the beams, whereas, vacuum chamber has a significant role in beam position monitoring, local pressure monitoring, temperature monitoring in beam duct, etc. As the two beams intersect each other at a large angle, the IR magnet can come much closure to the IP. High luminosity causes high beam-induced background, such as Touschek scattering, beam-gas scattering, Synchrotron scattering, radiative Bhabha scattering, pair photon production, etc.

2.2.2 Pixel Detector

The innermost detector is based on Depleted P-channel Field Effect Transistor (DEPFET) technology. It has two layers of 8 and 12 ladders with 40 sensors at 1.4 cm and 2.2 cm respectively. When a charged particle passes through PXD, it produces electron-hole pairs, which further generates electron drift into the internal gate generating a signal. Transistors amplified this signal above the threshold of the DAQ system (see

Figure 2.3). PXD uses an online data reduction system that figures out the ROI by extrapolating the tracks found in SVD. This process reduces the background hits a bit. So, PXD is necessary for vertex resolution and tracking, but the detection of low momentum particle that is unable to cross SVD properly is always challenging.

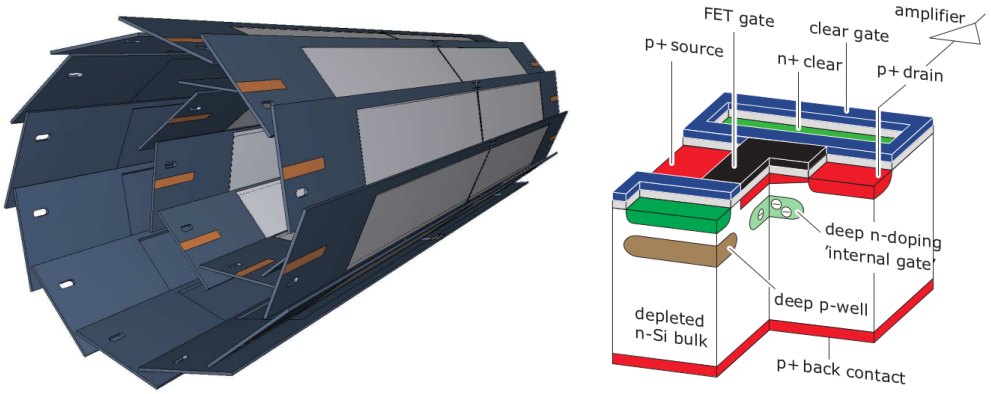

(a) Schematic arrangement of two layers in PXD (b) Working principle of DEPFET

Figure 2.3: Pixel Detector

2.2.3 Silicon Vertex Detector

SVD is highly responsible for detecting low momentum tracks. It is a kind of Double-sided strip detector (DSSD) which contains $P+$ and $N+$ silicon strip to provide $2D$ coordinate hits information (signal produced due to charge drift). The description of its layer arrangement is provided in table 2.1 and shown in Figure 2.4.

Layers	Position (cm)	No. of Ladders
Third	3.8	8
Fourth	8.0	10
Fifth	11.5	14
Sixth	14.0	17

Table 2.1: Simple layout of SVD

APV 2S is used as electronic signal readout chips. As the hits information is based on strip location, it contains Ghost hits [4] in addition to the beam background with

[4]Ghost hit: In 2D strip configuration we will get two false hits at the opposite diagonal of the original hits positions

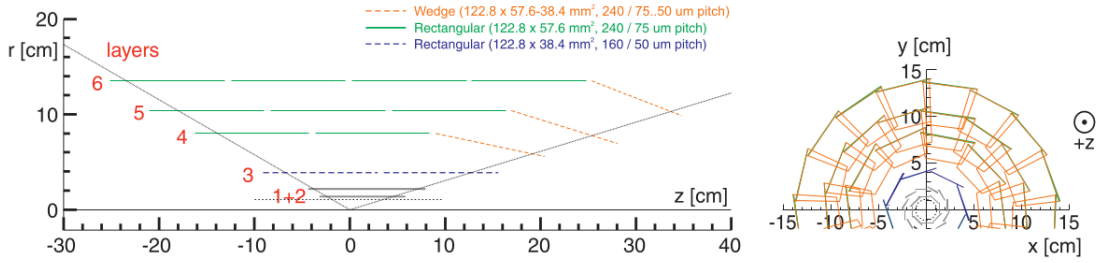

Figure 2.4: Layer arrangement of SVD

noise. All information on charge, hit time, and position are gathered from all strips to apply the clustering algorithm, which further helps to reconstruct tracks of the particle. These tracks are extrapolated in PXD to create ROI.

2.2.4 Central Drift Chamber

The main instrument of the Belle II spectrometer is the CDC. It has 9 super layers composed of 56 layers and 14336 wires. Layers are of two types: axial wire layer, where sense wire are parallel to the beam-line, and stereo wires layer, where sense wires are skewed to the beam-line. The Drift chamber is filled with $He - C_2H_6$ (50 : 50 mixture) with an average drift velocity of 3.3 cm μ s^{-1}. Charged traversing particles ionize gas molecules that eventually followed up in secondary ionization to produce an avalanche of electrons. These electron avalanche enough to generate a signal in the sense wires. CDC is responsible for reconstructing and measuring the momentum of charged tracks, particle identification from $\frac{dE}{dX}$ information and store trigger signals for charged particles.

2.2.5 Particle identification: Barrel

This region uses the time of propagation (TOP) counter to improve K/π separation. Likelihood of each particle at every detector provides the information of particle identification. Barrel region is composed of 16 quartz Cherenkov radiator bars (2.6 m $\times$ 45 cm $\times$ 2 cm) with spherical focusing mirror on one side and expansion prism and readout electronics on the other side (see Figure 2.5). Traversing charged particles

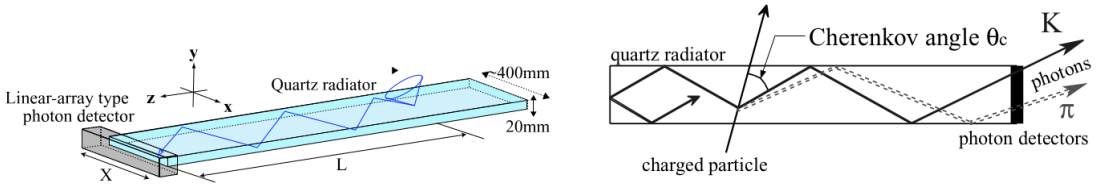

(a) Schematic diagram of the quartz bar (b) Working principle

Figure 2.5: Overview of TOP counter

emit Cherenkov [5] radiated photons, which further get internally reflected in the quartz bar to form a virtual image using the spherical focusing mirror. At the backside, the Cherenkov photon moves through a prism that expands the image of Cherenkov ring. After it falls on MCP-PMTS, it gives 2D position information of the Cherenkov ring and its time. That's why TOP requires high single-photon resolution ($< 100\,\text{ps}$).

2.2.6 Particle Identification: End Cap

Cherenkov photons radiate at a certain angle depending on the material's refractive index (n) and its velocity (v) as $\cos\theta = \frac{1}{nv}$ where $\beta = \frac{v}{c}$. Thus, it creates a ring like shape whose radius has information about the Cherenkov angle of radiation and particle velocity. RICH can be achieved in different mediums like gases, crystal, etc., but Aerogel is perfect for providing a higher refractive index , thickness and can cover a large solid angle. To increase light yield, Belle II uses two layers of Aerogel system (see Figure 2.6) with different refractive index ($n1 = 1.045$ and $n2 = 1.055$). A Hybrid avalanche photon detector (HAPD) can provide high single-photon sensitivity. This information is required to construct the likelihood hypothesis of the particle.

2.2.7 Electromagnetic Calorimeter

ECL detects photons and electrons and measures their energy and angular coordinates. Thallium doped CSI scintillator [6] is used to measure wide range of photon

[5] Cherenkov radiation: When particle travels through a dielectric medium at a higher velocity than the phase velocity of light in that medium, it emits electromagnetic radiation.

[6] Scintillator is a transparent material that emits light when the traversing particle ionized it.

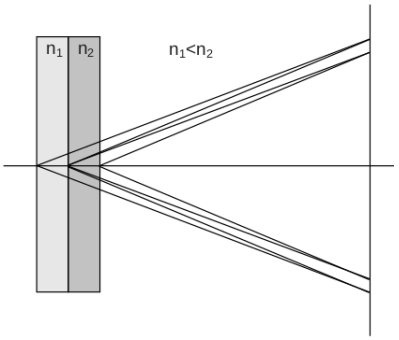

Figure 2.6: Two layers Aerogel system in ARICH

energy ($0.02 - 4\,\mathrm{GeV}$). Electron and photon lose energy by Bremsstrahlung and pair production respectively, whereas, hadrons lose energy mostly by ionization and inelastic scattering loss. Stopping power of muon in the Bethe region depends on minimum ionization (which is up to several GeV), that's why muon will traverse through all these detectors without losing much of its energy. In ECL, particle loses energy in a thunder-strike like pattern, known as the electromagnetic shower. Soft background photons are responsible for pile-up noises which are tackle with wave-form-sampling readout electronics. Readout system creates a grid of wave amplitudes that proceed with the clustering algorithm to identify it.

2.2.8 K_L^0 and μ detector

The outermost detector, which is responsible for detecting K_L^0 and muons, is located outside of superconducting solenoid. The barrel region has 15 layers with alternating 4.7 cm thick iron plates, whereas, the end cap has 14 layers with a similar pattern of iron plates. These iron plates have 3.9 interaction length [7] and help to return the magnetic flux of solenoid. Due to the high production of the neutron from the background showers, KLM uses scintillator strips with wavelength shifting fibers coupling and Silicon Photo Multiplier (SiPM). In these layers K_L^0 losses energy, and shows hadronic shower which further, gives information about the fake-pion rates. On the other hand, muon identification can be possible if its momentum is more than $0.7\,\mathrm{GeV}/c$. GEANT4 extrapolates tracks from the CDC of muon hits to KLM as muon passes

[7] Hadronic mean free path

through all inner detector without losing much of its energy and has the potential to traverse through KLM completely.

2.2.9 Detector Solenoid and Iron Structure

A NiTi/Cu superconducting solenoid presents between ECL and KLM in the barrel region. Its shape is cylindrical with a base radius of 1.7 m and a length of 4.4 m, which is enough to generate a magnetic field of 1.5 T. Magnetic flux return mechanisms are provided by iron plates and calorimeters. The iron yoke is the iron structure that returns magnetic flux and offers overall support to all detectors. Its barrel region is made up of 8 KLM layers and 200 mm alternating thick flux-return plates. This octagonal-shaped iron yoke is made up of $S10C$ iron with a dimension of 4.4 m $\times$ 7.7 m $\times$ 7.7 m.

2.2.10 Trigger System

High cross-section of Bhabha scattering and pair photons production requires a sophisticated trigger system to achieve high luminosity. Low-level hardware-based ($L1$) trigger and High-level software-based (HLT) trigger are the two components of the Belle II triggering system. Here, the $L1$ trigger composed of many sub-trigger systems whose composite signal is processed by the final part of the triggering system, known as Global Decision Logic (GDL). The following table 2.2 describes how sub-triggers are responsible for various information gathering.

Sub-trigger	**Information**
CDC	Momentum, Position, track count, charges of tracks etc.
Barrel PID	Hit timing , hit topology
Endcap PID	Hit timing
ECL	Energy cluster count and deposit, Bhabha , $\gamma\gamma$ events
KLM	Muon tracks

Table 2.2: $L1$ trigger system

2.2.11 Data Acquisition System

DAQ transfers all $L1$ triggered detector readout data to the storage system. Central components of the DAQ system are:

1. Belle2Link
2. COPPER
3. Event build system
4. High level trigger system

Chapter 3

Analysis

3.1 BASF2

Belle II Analysis Software Framework (BASF2) is the core software to accumulate all Belle II internal components and third-party external packages [Kuhr 19]. The code is written in `C++`, and the executable scripts are usually written in `Python 3`. `ROOT` is used for input and output storages. Each data processing codes are structured in the form of blocks, called `modules`. These `modules` can be linked with a common framework, known as `path`. In an executable script code, `modules` are linearly placed in '`the path`'. Each `module` has access to transfer data in or out from a common platform, called `Data store`.

3.2 Event Generation

B-factory uses `EvtGen` [Lange 01], a Monte Carlo event generator, to produce B and D mesons decay chains. Each mother and daughter particle acts as a decay 'node' in this generator, providing its decay amplitude and decay modes. A small list of generic decay modes is given in table 3.1. Decay amplitude helps to calculate maximum probability that is essential in the `EvtGen` algorithm to accept or reject a generated

decay chain. Information about particle properties like mass, decay width, spins, etc. are provided to `EvtGen`. It allows diverse decay model generations like generic decay, CP violation decay, semi-leptonic decay, etc. Descriptions of all our decay chains are listed in Appendix A.

Models	**Description**
PHSP	N-body phase space
SVS	Scalar decay to vector and scalar
VSS	Decays of vector particle to a pair of scalars
VSS_MIX	Decays a vector particle into two scalars ($\Upsilon(4S) \to B^0\bar{B}^0$ with $B^0 - \bar{B}^0$ mixing)
VLL	Decays of vector to two leptons

Table 3.1: List of generic models of `EvtGen` (used in our study)

3.3 Simulation

`GEANT4` package [Agostinelli 03] is used to simulate generated particles passing through the Belle II detector. `GEANT4` toolkit is written in the `C++` programming language and it facilitates most of the simulation involving particle interaction with matter. It can also run in a wide range of energy ($\sim$ MeV to $\sim$ GeV). High standard compatibility with event generator, reconstruction, and analysis components made `GEANT4` a perfect toolkit for detector simulation. It is capable to do:

1. Particle interaction with matter
2. Geometry
3. Digits and hits
4. Tracking
5. Track and event management
6. Visualization and its framework
7. User interface

3.4 Signal MC generation

We generated 1 Million Signal MC events for each of the decay modes of our interest (see table 3.2) at the resonance of $\Upsilon(4S)$ ($e^-e^+ \to \Upsilon(4S) \to B\bar{B}$, i.e., B^+B^- or $B^0\bar{B}^0$). Each mode includes its charge conjugate mode.

Sr No.	**Mode with decay chain**
1)	$B^+ \to \psi(2S)\, K^+$, $\psi(2S) \to \chi_{c1}\, \gamma$, $\chi_{c1} \to J/\psi\, \gamma$, $J/\psi \to \ell^+\, \ell^-$
2)	$B^+ \to X(3872)\, K^+$, $X(3872) \to \chi_{c1}\, \gamma$, $\chi_{c1} \to J/\psi\, \gamma$, $J/\psi \to \ell^+\, \ell^-$
3)	$B^+ \to X(3823)\, K^+$, $X(3823) \to \chi_{c1}\, \gamma$, $\chi_{c1} \to J/\psi\, \gamma$, $J/\psi \to \ell^+\, \ell^-$
4)	$B^0 \to \psi(2S)\, K^+\, \pi^-$, $\psi(2S) \to \chi_{c1}\, \gamma$, $\chi_{c1} \to J/\psi\, \gamma$, $J/\psi \to \ell^+\, \ell^-$
5)	$B^0 \to X(3872)\, K^+\, \pi^-$, $X(3872) \to \chi_{c1}\, \gamma$, $\chi_{c1} \to J/\psi\, \gamma$, $J/\psi \to \ell^+\, \ell^-$
6)	$B^0 \to X(3823)\, K^+\, \pi^-$, $X(3823) \to \chi_{c1}\, \gamma$, $\chi_{c1} \to J/\psi\, \gamma$, $J/\psi \to \ell^+\, \ell^-$

Table 3.2: Decay modes of our study (here, $\ell \in \{e, \mu\}$).

3.5 Reconstruction

Intermediate heavy particle sooner or later decays into its final state particles like $e^{\pm}$, $\mu^{\pm}$, $K^{\pm}$, $K^0_{S,L}$, $\pi^{\pm}$, π^0, p, d, and γ. We saw in the previous chapter how the detectors are designed to perceive these end state particles. With all simulation information of these particles, we can reconstruct our mother particles step by step. It can be represented as a tree structure where each leaf is a final state particle; branch is the intermediate short/long-lived heavy particle, and the stem is our B mesons. Before the process of combinations of different final state particles, we need to select these particles with different cuts [1]. We will discuss this specific selection region in the following section.

[1] Cut is the selection window of the measurement.

3.6 Particle Selection

In our study, charged hadrons ($\pi^{\pm}$, $K^{\pm}$), charged leptons ($e^{\pm}$, $\mu^{\pm}$) and neutral particles (γ) are the final daughter particles. We have already given some intuition in the previous chapter how different types of measurement involved to identify these particles. Also, aggregate information of many detectors and sub-detectors are required to construct the likelihood of each particle hypothesis (charged particle).

3.6.1 Charged Particles

- dE/dX measurement in SVD and CDC, time of flight (TOF) in TOP and number of Cherenkov photons in ARICH are the essential tools to separate pions and kaons. The likelihood ratio of kaons and pions

$$\mathcal{L}(a:b) = \frac{\mathcal{L}_a}{\mathcal{L}_a + \mathcal{L}_b}$$

  measures the efficiency and fake-pion rates. The efficiency of $K - \pi$ separation is better below $3\,\mathrm{GeV}/c^2$.

- The E/p value, where E is the energy measured in ECL and p is the momentum of the track, is the best way to distinguish electrons from other charged particles. Information of dE/dX, TOF, no. of Cherenkov photons are also required, but E/p ratio remains the primary source of electron identification.

- Muons mostly rely on the KLM detector's information, i.e., measurement of longitudinal penetration depth and transverse scattering of the extrapolate track (from CDC). However, low momentum muons that are unable to reach KLM are very challenging to separate from pions as they both show a similar pattern of dE/dX.

Tracks are selected and identified as the charged particles as per the following cuts:

1. Charged particle identification probability > 0.1 that means for electron

$$e_{PID} = \frac{\mathcal{L}_e}{\mathcal{L}_e + \mathcal{L}_\mu + \mathcal{L}_\pi + \mathcal{L}_K + \mathcal{L}_p + \mathcal{L}_d} > 0.1$$

2. As the charged particles are coming from B meson, they produced very close to IP. That's why the tracks are selected if they are within a transverse distance (dr, x-y plane) of $0.5\,cm$ from IP and $2\,cm$ in the beam direction (dz)

3. Particle is within CDC angular acceptance

4. Number of CDC hits associated with the tracks > 20.

3.6.2 Neutral Particle (γ)

Photons are identified in the ECL by their EM shower pattern. It has a significant cylindrical symmetric pattern of energy deposition. Primary selection measurement depends on the ratio of different grid areas of the crystal, like E_9/E_{25} or E_1/E_9 (E_{i^2} means the deposition of energy in the $i \times i$ crystal.

Photons are selected with the following cuts in our study:

1. Energy > 75 MeV

2. $E_1/E_9 > 0.4$

3. ECL cluster's timing uncertainty that contains 99% of true photons $< 1\,ms$

3.7 J/ψ

The above final state particles with their selective regions are combined to produce heavy intermediate particles. Lepton pairs are combined to reconstruct J/ψ. Figure

3.1 shows the invariant mass[2] histogram of $M(\ell\ell)$.

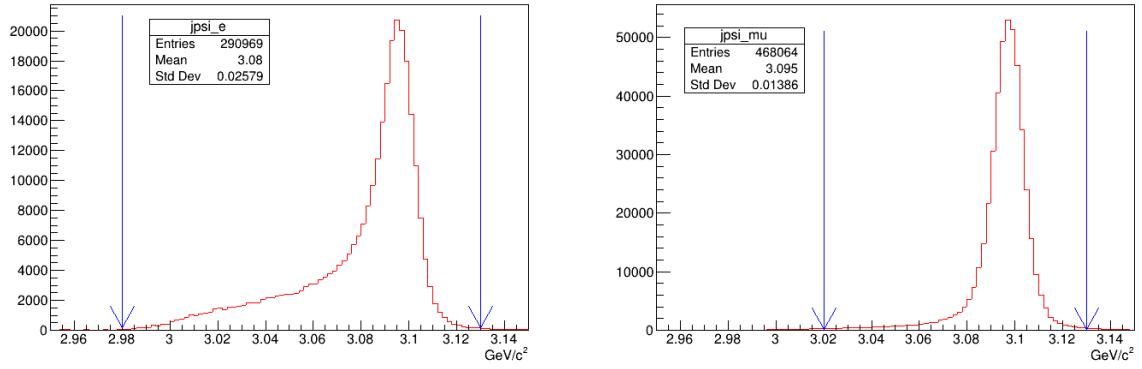

(a) $J/\psi \to e^- e^+$ (b) $J/\psi \to \mu^- \mu^+$

Figure 3.1: Invariant mass of reconstructed J/ψ, $M(\ell\ell)$ for $B^+ \to \psi(2S)\, K^+$ decay mode. Blue arrow is drawn to illustrate cut region.

Interestingly, the $M(e^-e^+)$ has a long tail pattern towards the lower mass. The loss of energy from electron in the form of Bremsstrahlung[3] photons are responsible for this kind of skewed shape. Due to the differences in J/ψ's plot, we applied different cuts to reconstruct higher tree elements.

- For $J/\psi \to e^- e^+$; selection criteria: $2.98 < M(e^-e^+) < 3.13\,\mathrm{GeV}/c^2$
- For $J/\psi \to \mu^- \mu^+$; selection criteria: $3.02 < M(\mu^-\mu^+) < 3.13\,\mathrm{GeV}/c^2$

3.8 χ_{c1}

χ_{c1} is reconstructed from photons and selected region of the reconstructed J/ψ. Figure 3.2 depicts the invariant mass spectrum of $M(J/\psi\gamma)$. Here we applied very loose cut (at the lower mass side) of $3.405 < M(j/\psi\gamma) < 3.550\,\mathrm{GeV}/c^2$.

[2]Invariant mass is calculated as $\sqrt{(\sum E_i)^2 + (\sum \overrightarrow{p}_i)^2}$, where E_i and $\overrightarrow{p}_i$ are the energy and the momentum of i^{th} daughter particle

[3]Bremsstrahlung is a process in which decelerated light charge particle, like electron, losses its energy in the form of radiated photons when it gets deflected by another charged particle.

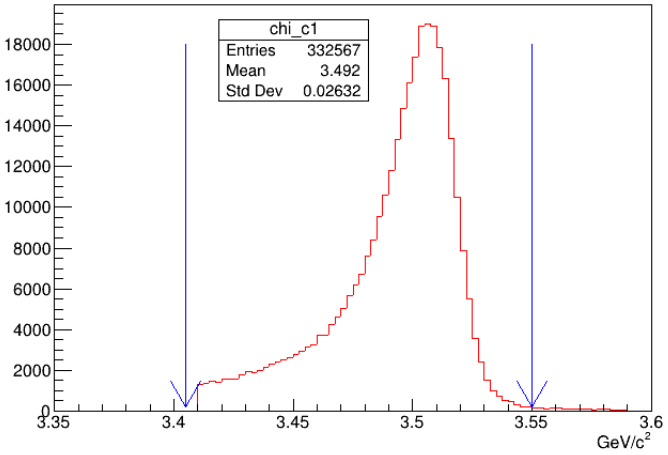

Figure 3.2: Invariant mass of reconstructed χ_{c1}, $M(J/\psi\gamma)$ for $B^+ \to \psi(2S)\, K^+$ decay mode. Blue arrow is drawn to illustrate cut region.

3.9 $\psi(2S)$, $X(3872, 3823)$ and B mesons

After the reconstruction of χ_{c1}, $\psi(2S)$ and $X(3872, 3823)$ are reconstructed by combining the photons with the selected region of χ_{c1}. Further, they combined with K and π (for three body decay) to reconstruct B mesons ($B^{\pm}, B^0$ and $\bar{B}^0$). Apart from the mass spectrum, ΔE and M_{bc} are two important variables to compare the reconstructed value with the expected one. Here,

$$\Delta E \equiv E_B - E_{Beam} \qquad \text{and} \qquad M_{bc} \equiv \sqrt{E_{beam}^2 - p_B^2}$$

where E_{beam} is the run time beam energy in the center mass frame, E_B and P_B are the energy and the magnitude of momentum of the reconstructed B mesons. As $e^- e^+ \to B\bar{B}$ meson pairs, ideally $\Delta E \approx 0$ and $M_{bc} \approx$ invariant mass of B mesons. ΔE and M_{bc} of $B \to \psi(2S)\, K$ decay mode are shown in figure 3.3. We selected signal window of ΔE and M_{bc} as $-0.2 < \Delta E < 0.05$ GeV and $M_{bc} > 5.27\,\text{GeV}/c^2$ respectively.

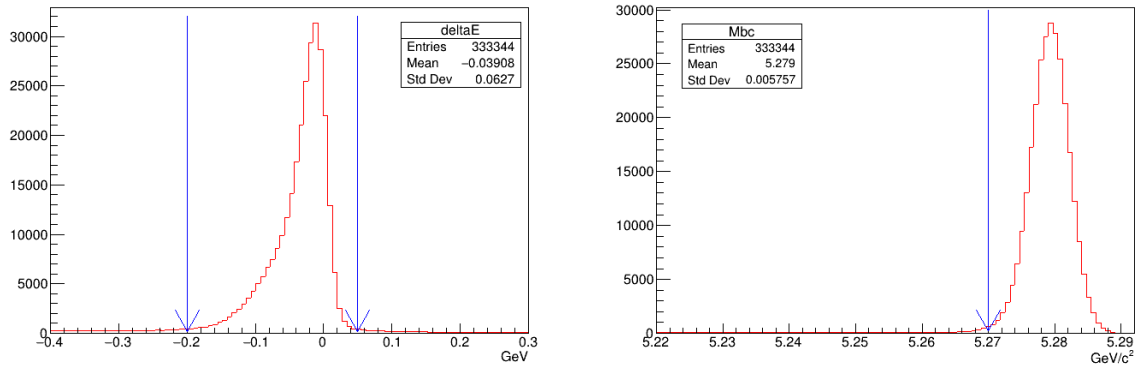

(a) ΔE (b) M_{bc}

Figure 3.3: ΔE and M_{bc} plots of $B^+ \to \psi(2S)\, K^+$ decay mode. Blue arrow is drawn to illustrate cut region.

3.10 Vertex Fitter

Vertex fitter rearranges vertices of decay chain at a common set of points, which means all daughter particles are produced at a common vertex of their mother particle. In our analysis, we used tree fitter (originated from BaBar collaboration) that modifies the entire decay chain with new fitting parameters. This optimization involves a goal of least square estimation of χ^2:

$$\chi^2 = (\overrightarrow{p} - \overrightarrow{h})M^{-1}(\overrightarrow{p} - \overrightarrow{h})^T$$

where, $\overrightarrow{p}$: parameters, $\overrightarrow{h}$: hypothesis, and M: Measurement co-variance. Tree fitter uses Kalman filter to reduce this time taken procedure (inverse of this huge matrix). Narrow peaks in J/ψ and χ_{c1} enable us to put a mass constraint on them. Then, their mass distribution forms a delta function peak; furthermore, this process improves our results.

3.11 Best Candidate Selection

In each event, we expect only one B mesons of interest to be reconstructed. However, due to combinations, one expects to have multiple B candidates. To remove the wrong

combination and select the true B candidate, we performed best candidate selection with χ^2 ranking.

$$\chi^2 = \left(\frac{M_{(J/\psi\gamma)} - m_{\chi_{c1}}}{\sigma_{(J/\psi\gamma)}}\right)^2 + \left(\frac{M_{(\ell\ell)} - m_{J/\psi}}{\sigma_{(\ell\ell)}}\right)^2 + \chi^2_{track} + \chi^2_{fitter}$$

where,

- For two body decay:
$$\chi^2_{track} = \left(\frac{M_{\ell\ell K} - m_{\ell\ell K}}{\sigma_{\ell\ell K}}\right)^2$$
- For three body decay:
$$\chi^2_{track} = \left(\frac{M_{\ell\ell K\pi} - m_{\ell\ell K\pi}}{\sigma_{\ell\ell K\pi}}\right)^2$$

Here, M is the reconstructed mass, m is the nominal mass, and σ is the standard deviation of the reconstructed mass. Based on this χ^2 value, we rank them from lower to higher order (see figure 3.4). Here, the "best candidate" is the particle list with the lowest χ^2 value or whose rank is 1. Figure 3.5 shows the contrast between the before and after effects of best candidate selection.

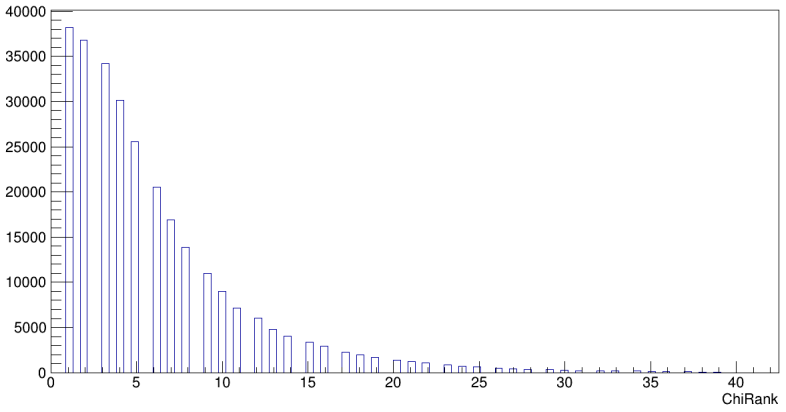

Figure 3.4: Rank of χ^2 of $B^+ \to \psi(2S)\, K^+$ decay mode. Here $\chi^2_{rank} = 1$ means our "best candidate".

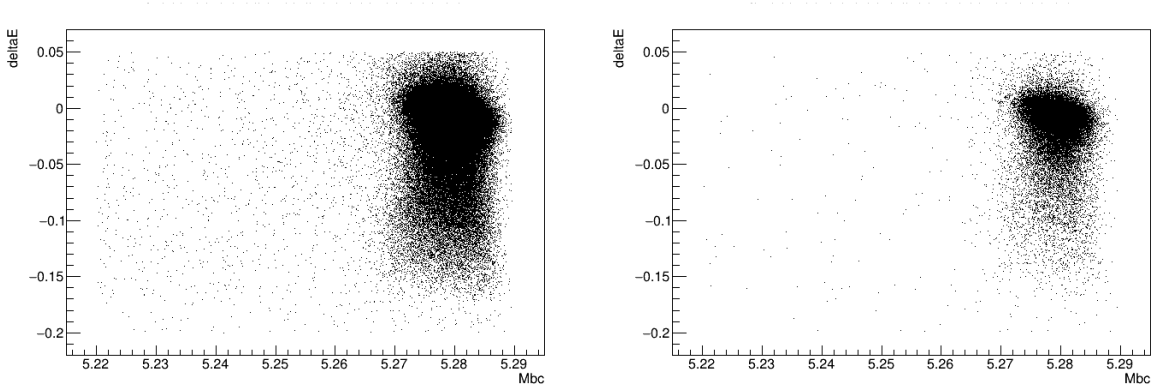

(a) Before best candidate selection

(b) After best candidate selection

Figure 3.5: ΔE vs M_{bc} plots of $B^+ \to \psi(2S)\, K^+$ decay mode. Each black dot represents our signal. Right plot shows our 'true' B candidates.

3.12 ΔE scaling

As one knows, photon detection is quite challenging aspects in the detector. Further, recovering the shower is not easy and generally results in energy loss leading to poor resolution. The same effect is reflected in our ΔE resolution. One can clearly see the tail on the left side of the ΔE distribution. Further, this also results in poor resolution in the M($\chi_{c1}\gamma$) distribution (used to identify the signal). In order to improve the resolution, we perform a trick (ΔE scaling). We assume that if we had adequately reconstructed the γ from the $X(3872)$, $X(3823)$, or $\psi(2S)$, then we should have ideally got ΔE to be zero. Assuming this, we force the ΔE to be zero by adjusting the four momenta of the photon. This scaled photon is then further utilized to reconstruct $M(\chi_{c1}\gamma)$. As one sees, we improve the resolution by this method (see Figure 3.8).

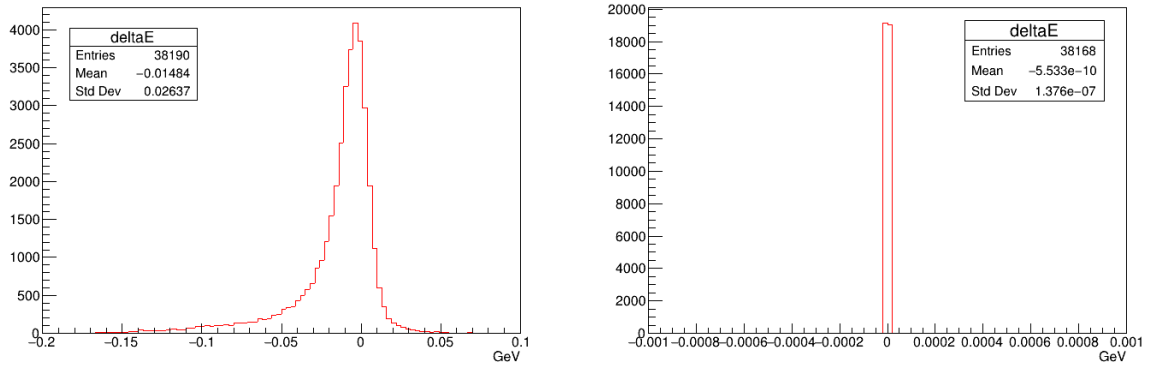

(a) Before ΔE scaling

(b) After ΔE scaling

Figure 3.6: ΔE plots of $B^+ \to \psi(2S)\, K^+$ decay mode.

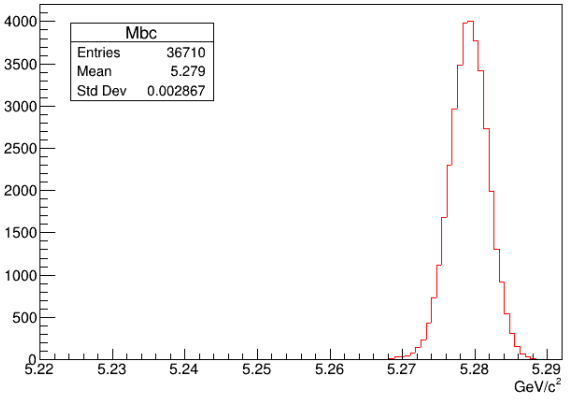

Figure 3.7: M_{bc} of $B^+ \to \psi(2S)\, K^+$ decay mode after ΔE scaling.

3.13 Background Study

The generic charged [4] MC is used to do the background study of $B^+ \to \psi(2S)\, K^+$ decay mode. Again, we reconstruct all the particles similarly, without ΔE scaling. Then we look at the M_{bc} and invariant mass of $\psi(2S)$ after removing the signal. While background M_{bc} is flat, however, the reconstructed mass of $\psi(2S)$ shows a peaking background around $3.53\,\mathrm{GeV}/c^2$ (see Figure 3.9).

[4] Generic charged MC is generated by the Belle II data production group (luminosity= $500\, fb^{-1}$). "Generic charged" reflects all decay modes of $e^- e^+ \to \Upsilon(4S) \to B^+ B^-$ channel.

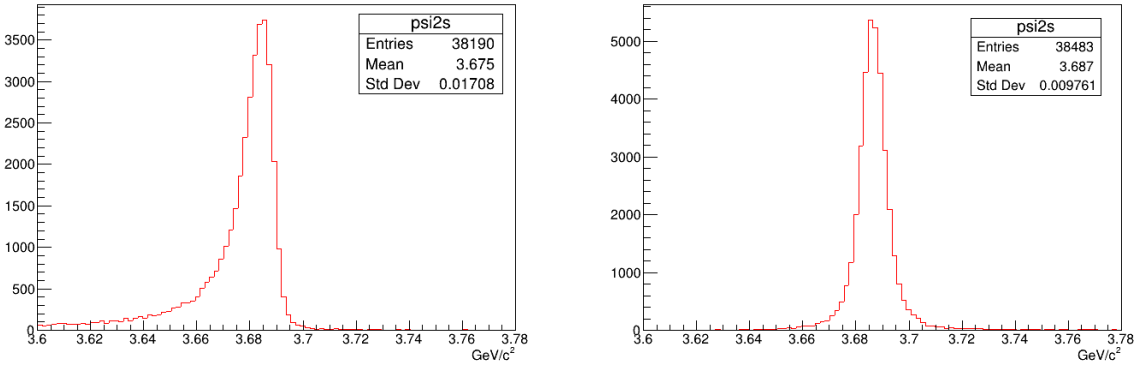

(a) Before ΔE scaling

(b) After ΔE scaling

Figure 3.8: Mass resolution of $(\chi_{c1}\gamma)$ of $B^+ \to \psi(2S)\, K^+$ decay.

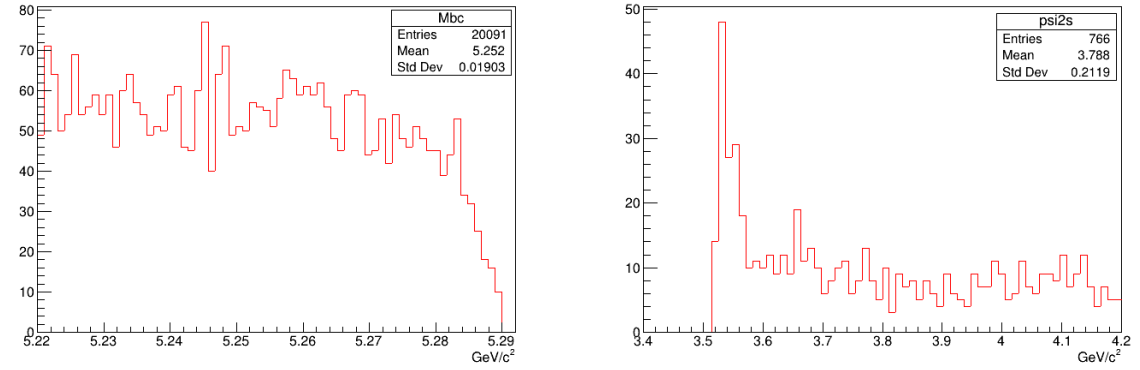

(a) Background M_{bc}

(b) Background $M(\chi_{c1}\gamma)$

Figure 3.9: Background plots after removing the signal of $B^+ \to \psi(2S)\, K^+$ decay mode.

First, we thought it was coming from $B^+ \to \psi(2S)\, K^{*+};\ K^{*+} \to K^+\, \pi^0;\ \pi^0 \to \gamma\gamma$. To check our guess, we reconstruct K^{*+} from the events, but it hasn't got any peak around its mass. Later, we tried to inspect the mother particle of the photons in our event. Interestingly, it (photon that decays from χ_{c1}) matches with π^0's PDG code (see Figure 3.10). It seems the background is coming from some random π^0. As the photon is decaying from π^0, one might need to apply the π^0 veto to reject this background.

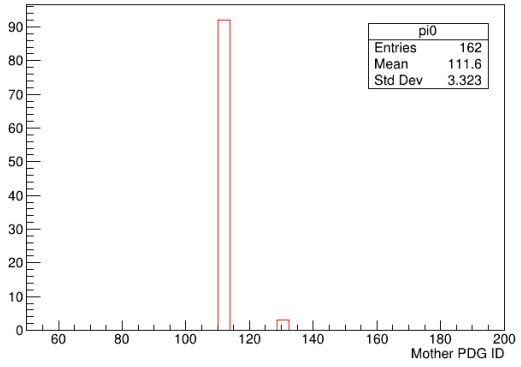

(a) PDG code of the mother particle

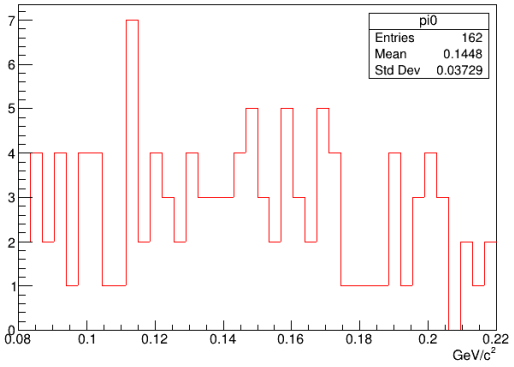

(b) Invariant mass of reconstructed π^0, $M(\gamma\gamma)$

Figure 3.10: PDG code of π^0 is 111 (left), but there is no peak at its mass (right) after putting a cut on $\psi(2S)$ mass: $M(\chi_{c1}\gamma) < 3.6\,\mathrm{GeV}/c^2$. This plot (right) is made with γ from χ_{c1}, but the π^0 might be made with other photons in the list.

Chapter 4

Result

4.1 Signal Efficiency

We performed every step of the reconstruction process that we have discussed in the previous chapter, with each decay mode. Now, we are interested in calculating the signal efficiency of all the decay modes.

$$\text{Efficiency} = \frac{\text{Signal Yield}}{\text{Total number of generated events}}$$

Here, We performed 1D unbinned maximum likelihood fit to estimate the signal yield or the number of reconstructed signal events. For M_{bc} plots, the sum of two Gaussian and Argus probability distribution functions (PDF) is used (see figure 4.1). Signal efficiency is provided in Table 4.1. Efficiency of the two body decay mode is almost 2.3 times more than the three body decay mode.

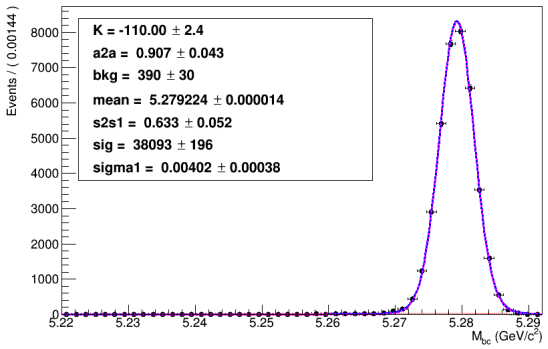

$B^+ \to \psi(2S)\, K^+$

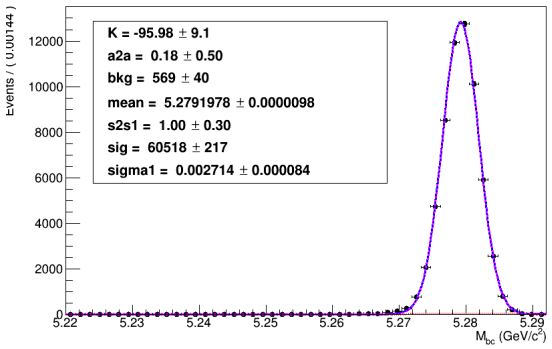

$B^+ \to X(3823)\, K^+$

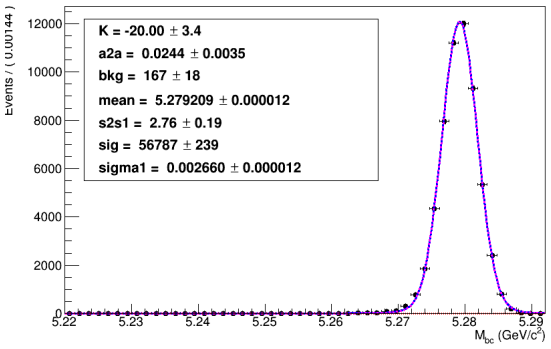

$B^+ \to X(3872)\, K^+$

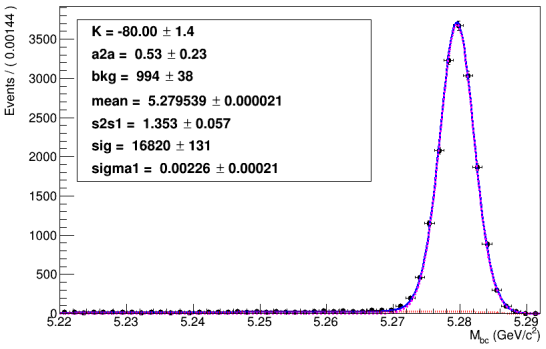

$B^0 \to \psi(2S)\, K^+\, \pi^-$

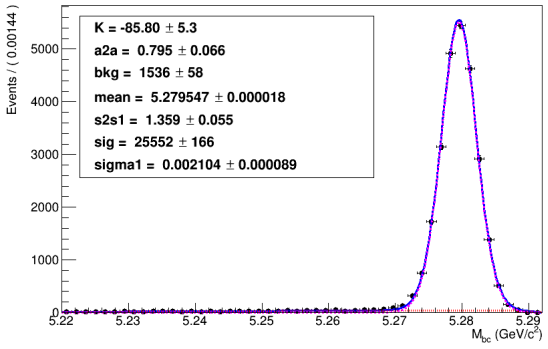

$B^0 \to X(3823)\, K^+\, \pi^-$

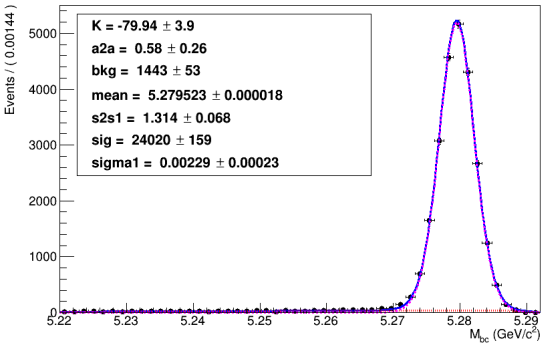

$B^0 \to X(3872)\, K^+\, \pi^-$

Figure 4.1: 1D UML fit of M_{bc} of all decay modes. Blue line is for the combined pdf, magenta is for the sum of two Gaussian and red is for the Argus. 'sig' parameter gives the signal yield.

Decay Modes	**Efficiency** (in %)
$B^+ \to \psi(2S)\, K^+$	3.81 ± 0.02
$B^0 \to \psi(2S)\, K^+\, \pi^-$	1.68 ± 0.01
$B^+ \to X(3823)\, K^+$	6.05 ± 0.02
$B^0 \to X(3823)\, K^+\, \pi^-$	2.56 ± 0.02
$B^+ \to X(3872)\, K^+$	5.68 ± 0.02
$B^0 \to X(3872)\, K^+\, \pi^-$	2.40 ± 0.02

Table 4.1: Signal reconstruction efficiency for the decay mode of interest.

4.2 Reconstructed mass of ($\chi_{c1}\gamma$)

As we planned to identify our signal using $M(\chi_{c1}\gamma)$, we performed 1D unbinned maximum likelihood fit to look at the final mass resolution of $X(3823)$ and $X(3872)$. This fit uses the combination of three Gaussian probability distribution functions. Figure 4.2 shows all the fitted plots and table 4.2 provides the list of the mass of reconstructed particles.

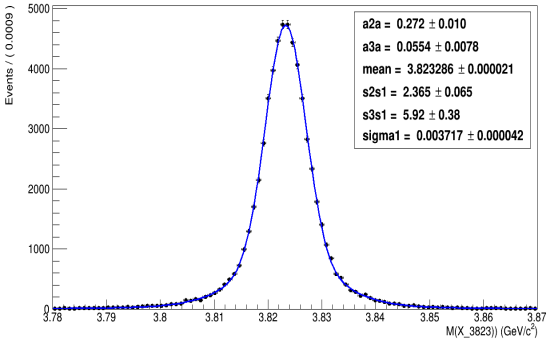

$B^+ \to X(3823)\, K^+$

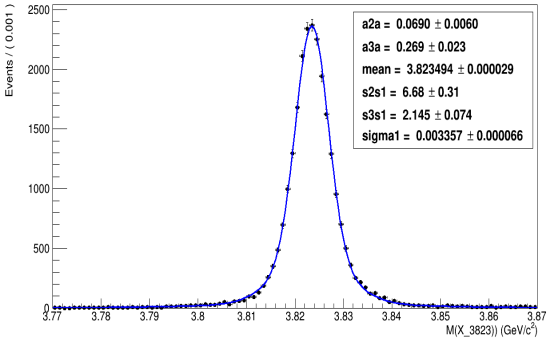

$B^+ \to X(3823)\, K^+\, \pi^-$

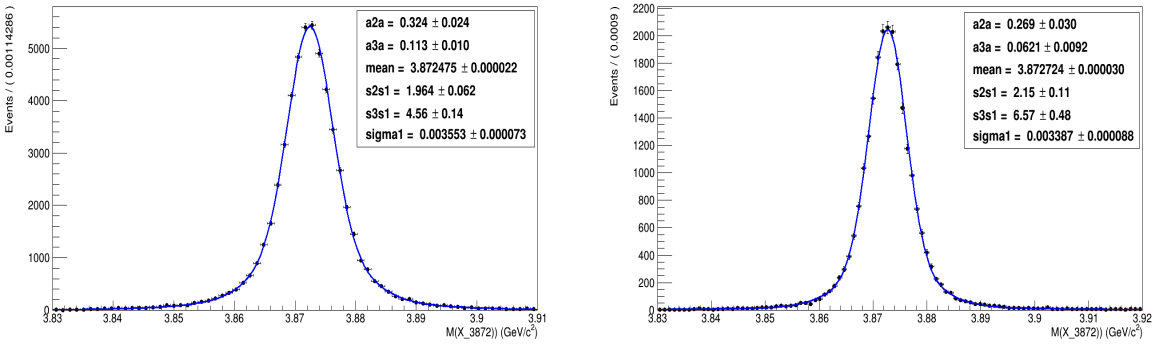

$B^+ \to X(3872)\, K^+$ $B^0 \to X(3872)\, K^+\, \pi^-$

Figure 4.2: 1D UML fit of $M(\chi_{c1}\gamma)$ of each decay mode

Decay Mode	**Reconstructed $M(\chi_{c1}\gamma)$ (GeV/c^2)**	
	Mean	Std. deviation
$B^+ \to X(3823)\, K^+$	3.823	0.006 ± 0.001
$B^+ \to X(3823)\, K^+\, \pi^-$	3.823	0.005 ± 0.001
$B^+ \to X(3872)\, K^+$	3.872	0.007 ± 0.001
$B^0 \to X(3872)\, K^+\, \pi^-$	3.873	0.005 ± 0.001

Table 4.2: List of the mass of reconstructed $X(3823)$ and $X(3872)$ in different decay modes.

Summary

We made a very basic selection of the events for the $B \to (\chi_{c1}\gamma)K$ and $B \to (\chi_{c1}\gamma)K\pi$ decay modes. We improved the resolution of $M(\chi_{c1}\gamma)$ using ΔE scaling. While studying the background, a possible source is seen from a random π^0, s photon, which one can remove by using the π^0 veto. Further, we estimated the signal efficiency using basic cuts and criteria. We were not able to achieve what was thought for this project due to the COVID19 situation. But we are somewhat close to it.

Further, work is needed to optimize the cuts and reduce the background to have better sensitivity for this analysis

Decay Modes	**Efficiency** (%)
$B^+ \to \psi(2S)\, K^+$	3.81 ± 0.02
$B^0 \to \psi(2S)\, K^+\, \pi^-$	1.68 ± 0.01
$B^+ \to X(3823)\, K^+$	6.05 ± 0.02
$B^0 \to X(3823)\, K^+\, \pi^-$	2.56 ± 0.02
$B^+ \to X(3872)\, K^+$	5.68 ± 0.02
$B^0 \to X(3872)\, K^+\, \pi^-$	2.40 ± 0.02

Table: Signal reconstruction efficiency of the decay modes of interest. These numbers are taken from the 1D UML fit to the M_{bc} distribution.

Appendix A

Decay File

A.1 Decay file for two body decay

A.1.1 $\psi(2S)$

Alias MyB+ B+
Alias MyB- B-
Alias Mychi chi_c1
Alias Mypsi Jpsi

Decay Upsilon(4S)
0.5 MyB+ B- VSS;
0.5 B+ MyB- VSS;
Enddecay

Decay MyB+
1.0 psi(2S) K+ SVS;
Enddecay

```
Decay MyB-
1.0 psi(2S) K- SVS;
Enddecay


Decay psi(2S)
1.0 Mychi gamma PHSP;
Enddecay


Decay Mychi
1.0 Mypsi gamma PHSP;
Enddecay


Decay Mypsi
0.5 e+ e- VLL;
0.5 mu+ mu- VLL;
Enddecay


    End
```

A.1.2 $X(3823)$

```
Alias MyB+ B+
Alias MyB- B-
Alias Mychi chi_c1
Alias Mypsi Jpsi


Decay Upsilon(4S)
0.5 MyB+ B- VSS;
0.5 B+ MyB- VSS;
```

```
Enddecay

Decay MyB+
1.0 X3823 K+ SVS;
Enddecay

Decay MyB-
1.0 X3823 K- SVS;
Enddecay

Decay X3823
1.0 Mychi gamma PHSP;
Enddecay

Decay Mychi
1.0 Mypsi gamma PHSP;
Enddecay

Decay Mypsi
0.5 e+ e- VLL;
0.5 mu+ mu- VLL;
Enddecay

End
```

A.1.3 $X(3872)$

Alias MyB+ B+
Alias MyB- B-
Alias Mychi chi_c1
Alias Mypsi Jpsi

Decay Upsilon(4S)
0.5 MyB+ B- VSS;
0.5 B+ MyB- VSS;
Enddecay

Decay MyB+
1.0 X_1(3872) K+ SVS;
Enddecay

Decay MyB-
1.0 X_1(3872) K- SVS;
Enddecay

Decay X_1(3872)
1.0 Mychi gamma PHSP;
Enddecay

Decay Mychi
1.0 Mypsi gamma PHSP;
Enddecay

Decay Mypsi

0.5 e+ e- VLL;
0.5 mu+ mu- VLL;
Enddecay

End

A.2 Decay file for three body decay

A.2.1 $\psi(2S)$

Define dm 0.507e12

Alias MyB0 B0
Alias MyantiB0 anti-B0
Alias Mychi chi_c1
Alias Mypsi Jpsi

Decay Upsilon(4S)
0.5 MyB0 anti-B0 VSS_MIX dm;
0.5 B0 MyantiB0 VSS_MIX dm;
Enddecay

Decay MyB0
1.0 psi(2S) K+ pi- PHSP;
Enddecay

Decay MyantiB0
1.0 psi(2S) K- pi+ PHSP;

```
Enddecay


Decay psi(2S)
1.0 Mychi gamma PHSP;
Enddecay


Decay Mychi
1.0 Mypsi gamma PHSP;
Enddecay


Decay Mypsi
0.5 e+ e- VLL;
0.5 mu+ mu- VLL;
Enddecay


    End
```

A.2.2 $X(3823)$

```
Define dm 0.507e12


Alias MyB0 B0
Alias MyantiB0 anti-B0
Alias Mychi chi_c1
Alias Mypsi Jpsi


Decay Upsilon(4S)
0.5 MyB0 anti-B0 VSS_MIX dm;
```

0.5 B0 MyantiB0 VSS_MIX dm;
Enddecay

Decay MyB0
1.0 X3823 K+ pi- PHSP;
Enddecay

Decay MyantiB0
1.0 X3823 K- pi+ PHSP;
Enddecay

Decay X3823
1.0 Mychi gamma PHSP;
Enddecay

Decay Mychi
1.0 Mypsi gamma PHSP;
Enddecay

Decay Mypsi
0.5 e+ e- VLL;
0.5 mu+ mu- VLL;
Enddecay

End

A.2.3 $X(3872)$

Define dm 0.507e12

Alias MyB0 B0
Alias MyantiB0 anti-B0
Alias Mychi chi_c1
Alias Mypsi Jpsi

Decay Upsilon(4S)
0.5 MyB0 anti-B0 VSS_MIX dm;
0.5 B0 MyantiB0 VSS_MIX dm;
Enddecay

Decay MyB0
1.0 X_1(3872) K+ pi- PHSP;
Enddecay

Decay MyantiB0
1.0 X_1(3872) K- pi+ PHSP;
Enddecay

Decay X_1(3872)
1.0 Mychi gamma PHSP;
Enddecay

Decay Mychi
1.0 Mypsi gamma PHSP;
Enddecay

Decay Mypsi
0.5 e+ e- VLL;
0.5 mu+ mu- VLL;
Enddecay

End

Bibliography

[Aaij 12] R Aaij & *et al.* (LHCb Collaboration). *Observation of* $X(3872)$ *production in pp collisions at* $\sqrt{s} = 7 \sim$ *TeV* . The European Physical Journal C, vol. 72, no. 5, page 1972, 2012.

[Aaij 13] R Aaij & *et al.* (LHCb Collaboration). *Determination of the X (3872) meson quantum numbers*. Physical review letters, vol. 110, no. 22, page 222001, 2013.

[Aaij 20] R. Aaij & *et al.* (LHCb collaboration). *Study of the* $\psi_2(3823)$ *and* $\chi_{c1}(3872)$ *states in* $B^+ \to \left(J/\psi\pi^+\pi^-\right) K^+$ *decays*. arXiv:2005.13422, 2020.

[Abazov 04] VM Abazov & *et al.* (D0 Collaboration). *Observation and Properties of the* $X(3872)$ *Decaying to* $J/\psi\,\pi^+\,\pi^-$ *in* $p\bar{p}$ *Collisions at* $s = 1.96$ *TeV*. Physical review letters, vol. 93, no. 16, page 162002, 2004.

[Abe 02] Kazuo Abe & *et al. Observation of* χ_{c_2} *Production in B Meson Decay*. Physical review letters, vol. 89, no. 1, page 011803, 2002.

[Abe 05] Kazuo Abe & *et al.* (The Belle Collaboration). *Evidence for* $X(3872) \to \gamma\, J/\psi$ *and the sub-threshold decay* $X(3872) \to \omega\, J/\psi$. arXiv preprint hep-ex/0505037, 2005.

[Abe 10] Tetsuo Abe & *et al. Belle II technical design report*. arXiv preprint arXiv:1011.0352, 2010.

[Ablikim 15] M Ablikim & *et al.* (BESIII Collaboration). *Observation of the* $\psi(1\,3_2^D)$ *State in* $e^+e^- \to \pi^+\,\pi^-\,\gamma\,\chi_{c_1}$ *at BESIII*. Physical review letters, vol. 115, no. 1, page 011803, 2015.

[Abulencia 06] A Abulencia & *et al.* (CDF Collaboration). *Measurement of the dipion mass spectrum in* $X(3872) \to J/\psi\,\pi^+\,\pi^-$ *decays*. Physical review letters, vol. 96, no. 10, page 102002, 2006.

[Abulencia 07] A Abulencia & *et al.* (CDF Collaboration). *Analysis of the Quantum Numbers* J^{PC} *of the* $X(3872)$ *Particle*. Physical review letters, vol. 98, no. 13, page 132002, 2007.

[Acosta 04] Darin Acosta & *et al.* (CDF II Collaboration). *Observation of the Narrow State* $X(3872) \to J/\psi\,\pi^+\,\pi^-$ *in* $\bar{p}p$ *Collisions at* $s = 1.96$ *TeV*. Physical review letters, vol. 93, no. 7, page 072001, 2004.

[Agostinelli 03] S. Agostinelli. *GEANT4—a simulation toolkit*. Nuclear Instruments and Methods in Physics Research Section A: Accelerators, Spectrometers, Detectors and Associated Equipment, vol. 506, 2003.

[Antoniazzi 94] L Antoniazzi & *et al.* *Search for hidden charm states decaying into* J/ψ *or* ψ*'plus pions*. Physical Review D, vol. 50, no. 7, page 4258, 1994.

[Aubert 03] Bernard Aubert & *et al.* *Study of inclusive production of charmonium mesons in B decays*. Physical Review D, vol. 67, no. 3, page 032002, 2003.

[Aubert 05] Bernard Aubert & *et al.* (BABAR Collaboration). *Study of the* $B^- \to J/\psi\,K^-\,\pi^+\,\pi^-$ *decay and measurement of the* $B^- \to X(3872)\,K^-$ *branching fraction*. Physical Review D, vol. 71, no. 7, page 071103, 2005.

[Aubert 08] Bernard Aubert & *et al.* (BABAR Collaboration). *Observation of* $Y(3940) \to J/\psi\,\omega$ *in* $B \to J/\psi\,\omega\,K$ *at BABAR*. Physical review letters, vol. 101, no. 8, page 082001, 2008.

[Aubert 09] Bernard Aubert & *et al.* (BABAR Collaboration). *Evidence for* $X(3872) \to \psi(2S)\,\gamma$ *in* $B^{\pm} \to X(3872)\,K^{\pm}$ *decays and a Study of* $B \to c\bar{c}\,\gamma\,K$. Physical review letters, vol. 102, no. 13, page 132001, 2009.

[Barnes 05] T Barnes, Stephen Godfrey & ES Swanson. *Higher charmonia*. Physical Review D, vol. 72, no. 5, page 054026, 2005.

[Bhardwaj 11] V Bhardwaj & *et al.* (Belle Collaboration). *Observation of* $X(3872) \to J/\psi\,\gamma$ *and Search for* $X(3872) \to \psi\,\gamma$ *in B Decays*. Physical review letters, vol. 107, no. 9, page 091803, 2011.

[Bhardwaj 13a] V Bhardwaj & *et al.* (Belle Collaboration). *Evidence of a New Narrow Resonance Decaying to* $\chi_{c_1}\,\gamma$ *in* $B \to \chi_{c_1}\,\gamma\,K$. Physical review letters, vol. 111, no. 3, page 032001, 2013.

[Bhardwaj 13b] Vishal Bhardwaj. *Study of inclusive and exclusive multibody* B *decays to* χ_{c1} *and* χ_{c2} *mesons*. PoS, vol. Hadron2013, page 051, 2013.

[Bhardwaj 16] V. Bhardwaj & *et al.* (Belle collaboration). *Inclusive and exclusive measurements of* B *decays to* χ_{c1} *and* χ_{c2} *at Belle*. Physical Review D, vol. 93, page 052016, Mar 2016.

[Blank 11] M Blank & A Krassnigg. *Bottomonium in a Bethe-Salpeter-equation study*. Physical Review D, vol. 84, no. 9, page 096014, 2011.

[Chatrchyan 13] Serguei Chatrchyan & *et al.* (CMS collaboration). *Measurement of the* $X(3872)$ *production cross section via decays to* $J/\psi\,\pi^{+}\,\pi^{-}$ *in pp collisions at* $\sqrt{s} = 7$ *TeV*. Journal of High Energy Physics, vol. 2013, no. 4, page 154, 2013.

[Choi 03] S-K Choi & *et al.* (Belle Collaboration). *Observation of a narrow charmoniumlike state in exclusive* $B^{\pm} \to K^{\pm}\,\pi^{+}\,\pi^{-}\,J/\psi$ *decays*. Physical review letters, vol. 91, no. 26, page 262001, 2003.

[Choi 11] S-K Choi & *et al.* (Belle Collaboration). *Bounds on the width, mass difference and other properties of* $X(3872) \to \pi^{+}\,\pi^{-}\,J/\psi$ *decays*. Physical Review D, vol. 84, no. 5, page 052004, 2011.

[Close 08] Frank Close. *Three flavours of Hybrid or π exchange: which is more attractive?* arXiv preprint arXiv:0801.2646, 2008.

[del Amo Sanchez 10] Pablo del Amo Sanchez & *et al.* (BABAR Collaboration). *Evidence for the decay $X(3872) \to J/\psi\,\omega$.* Physical Review D, vol. 82, no. 1, page 011101, 2010.

[Ebert 03] D Ebert, RN Faustov & VO Galkin. *Properties of heavy quarkonia and B c mesons in the relativistic quark model.* Physical Review D, vol. 67, no. 1, page 014027, 2003.

[Eichten 02] Estia J Eichten, Kenneth Lane & Chris Quigg. *B-meson gateways to missing charmonium levels.* Physical review letters, vol. 89, no. 16, page 162002, 2002.

[Eichten 04] Estia J Eichten, Kenneth Lane & Chris Quigg. *Charmonium levels near threshold and the narrow state $X(3872) \to \pi^+\,\pi^-\,J/\psi$.* Physical Review D, vol. 69, no. 9, page 094019, 2004.

[Ericson 93] Torleif EO Ericson & Gabriel Karl. *Strength of pion exchange in hadronic molecules.* Physics Letters B, vol. 309, no. 3-4, pages 426–430, 1993.

[Gell-Mann 64] Murray Gell-Mann. *A Schematic Model of Baryons and Mesons.* Phys. Lett., vol. 8, pages 214–215, 1964.

[Godfrey 85] Stephen Godfrey & Nathan Isgur. *Mesons in a relativized quark model with chromodynamics.* Physical Review D, vol. 32, no. 1, page 189, 1985.

[Godfrey 08] Stephen Godfrey & Stephen L Olsen. *The exotic XYZ charmonium-like mesons.* Annual Review of Nuclear and Particle Science, vol. 58, pages 51–73, 2008.

[Herb 77] S. W. Herb. *Observation of a Dimuon Resonance at* 9.5 *GeV in* $400-$*GeV Proton-Nucleus Collisions.* Phys. Rev. Lett., vol. 39, pages 252–255, Aug 1977.

[Isgur 85] Nathan Isgur & Jack Paton. *Flux-tube model for hadrons in QCD.* Physical Review D, vol. 31, no. 11, page 2910, 1985.

[Ko 97] Pyungwon Ko, Jungil Lee & HS Song. *Color-octet mechanism in the inclusive D-wave charmonium productions in B decays*. Physics Letters B, vol. 395, no. 1-2, pages 107–112, 1997.

[Kou 19] Emi Kou & *et al.* *The Belle II physics book*. Progress of Theoretical and Experimental Physics, vol. 2019, no. 12, page 123C01, 2019.

[Kuhr 19] T Kuhr & *et al.* *The Belle II core software*. Computing and Software for Big Science, vol. 3, no. 1, page 1, 2019.

[Kwong 87] Waikwok Kwong, Jonathan L Rosner & Chris Quigg. *Heavy-quark systems*. Annual Review of Nuclear and Particle Science, vol. 37, no. 1, pages 325–382, 1987.

[Lange 01] David J Lange. *The EvtGen particle decay simulation package*. Nuclear Instruments and Methods in Physics Research Section A: Accelerators, Spectrometers, Detectors and Associated Equipment, vol. 462, no. 1-2, pages 152–155, 2001.

[Maiani 05] Luciano Maiani & *et al.* *Diquark-antidiquark states with hidden or open charm and the nature of* $X(3872)$. Physical Review D, vol. 71, no. 1, page 014028, 2005.

[Olsen 16] Stephen Lars Olsen. *A new hadron spectroscopy*. In AIP Conference Proceedings, volume 1701, page 050017. AIP Publishing LLC, 2016.

[Qiao 97] Cong-Feng Qiao, Feng Yuan & Kuang-Ta Chao. *Crucial test for the color-octet production mechanism in Z 0 decays*. Physical Review D, vol. 55, no. 7, page 4001, 1997.

[Swanson 06] Eric S Swanson. *The new heavy mesons: a status report*. Physics Reports, vol. 429, no. 5, pages 243–305, 2006.

[Törnqvist 94] Nils A Törnqvist. *From the deuteron to deusons, an analysis of deuteronlike meson-meson bound states*. Zeitschrift für Physik C Particles and Fields, vol. 61, no. 3, pages 525–537, 1994.

[Zyla 20] P.A. Zyla & *et al.* *Particle Data Group*. 2020.